

# Dynamics of clathrin-mediated endocytosis and its requirement for organelle biogenesis in *Dictyostelium*

Laura Macro, Jyoti K. Jaiswal\* and Sanford M. Simon<sup>‡</sup>

Laboratory of Cellular Biophysics, The Rockefeller University, New York, NY 10065, USA

\*Present address: Center for Genetic Medicine Research, Children's National Medical Center, Washington DC, DC 20010, USA

<sup>‡</sup>Author for correspondence ([simon@rockefeller.edu](mailto:simon@rockefeller.edu))

Accepted 21 August 2012

Journal of Cell Science 125, 5721–5732

© 2012. Published by The Company of Biologists Ltd

doi: 10.1242/jcs.108837

## Summary

The protein clathrin mediates one of the major pathways of endocytosis from the extracellular milieu and plasma membrane. In single-cell eukaryotes, such as *Saccharomyces cerevisiae*, the gene encoding clathrin is not an essential gene, raising the question of whether clathrin conveys specific advantages for multicellularity. Furthermore, in contrast to mammalian cells, endocytosis in *S. cerevisiae* is not dependent on either clathrin or adaptor protein 2 (AP2), an endocytic adaptor molecule. In this study, we investigated the requirement for components of clathrin-mediated endocytosis (CME) in another unicellular organism, the amoeba *Dictyostelium*. We identified a heterotetrameric AP2 complex in *Dictyostelium* that is similar to that which is found in higher eukaryotes. By simultaneously imaging fluorescently tagged clathrin and AP2, we found that, similar to higher eukaryotes, these proteins colocalized to membrane puncta that move into the cell together. In addition, the contractile vacuole marker protein, dajumin-green fluorescent protein (GFP), is trafficked via the cell membrane and internalized by CME in a clathrin-dependent, AP2-independent mechanism. This pathway is distinct from other endocytic mechanisms in *Dictyostelium*. Our finding that CME is required for the internalization of contractile vacuole proteins from the cell membrane explains the contractile vacuole biogenesis defect in *Dictyostelium* cells lacking clathrin. Our results also suggest that the machinery for CME and its role in organelle maintenance appeared early during eukaryotic evolution. We hypothesize that dependence of endocytosis on specific components of the CME pathway evolved later, as demonstrated by internalization independent of AP2 function.

**Key words:** Clathrin, AP2, *Dictyostelium*

## Introduction

Clathrin-mediated endocytosis (CME) is one of the major mechanisms for internalization of nutrients, signaling molecules and transmembrane receptors from the extracellular milieu and plasma membrane (McMahon and Boucrot, 2011). Although clathrin is required in metazoans, the gene encoding clathrin is not an essential gene in single-cell eukaryotes, such as *Saccharomyces cerevisiae* and *Dictyostelium* (Payne and Schekman, 1985; Lemmon and Jones, 1987; O'Halloran and Anderson, 1992; Ruscetti et al., 1994) raising the question of whether clathrin conveys specific advantages for multicellularity. In this study, we investigated the process of CME in *Dictyostelium*, a unicellular organism that can transition between a single-celled and differentiated multicellular form.

Clathrin functions by forming a polyhedral lattice that acts as a scaffold for vesicle formation. Given that clathrin itself is unable to bind to either the membrane or the cargo molecules that are to be transported, it requires adaptor proteins that can perform this function (Owen et al., 2004). One of the central adaptors for CME is the adaptor protein 2 (AP2) complex, which is a member of a family of protein complexes (AP1–AP4), each of which acts at different intracellular locations (Owen et al., 2004). The AP2 complex functions at the plasma membrane, where it selects cargo proteins based on sorting signals in their cytosolic tails (Ohno et al., 1995). The AP2 complex is a heterotetramer comprising two large subunits ( $\alpha$  and  $\beta$ 2), a medium subunit ( $\mu$ 2) and a small subunit ( $\sigma$ 2), which bind to each other with high

affinity (Collins et al., 2002). The ability of AP2 to bind simultaneously to cargo proteins, plasma membrane PI-(4,5)-P<sub>2</sub> and clathrin makes it an important 'hub' molecule for CME (Praefcke et al., 2004).

Genetic deletions of clathrin in *Dictyostelium* have revealed its importance for macropinocytosis, cytokinesis, development and osmoregulation (O'Halloran and Anderson, 1992; Ruscetti et al., 1994; Niswonger and O'Halloran, 1997a; Niswonger and O'Halloran, 1997b; Wang et al., 2003). Given that clathrin functions at numerous membrane transport steps, it has been difficult to resolve whether CME from the plasma membrane is important for any of these processes.

Evidence for CME in *Dictyostelium* is based on the observation that clathrin forms plasma membrane puncta that colocalize with AP2, epsin, Hip1r and AP180 (Stavrou and O'Halloran, 2006; Repass et al., 2007; Brady et al., 2008; Wen et al., 2009; Sosa et al., 2012). In the case of AP2, immunofluorescence studies using an antibody to the  $\alpha$  or  $\beta$ 1/2 subunits showed that they localize to clathrin puncta (Wen et al., 2009; Sosa et al., 2012). In addition, the  $\beta$ 1/2 subunit has been shown to interact with the  $\mu$ 2 subunit (Sosa et al., 2012); however, the existence of a full heterotetrameric AP2 complex similar to that found in mammalian cells has not been established.

In *Dictyostelium*, clathrin puncta have been observed to disappear at the plasma membrane coincident with a burst of actin (Brady et al., 2010). Although disappearance of clathrin from the membrane is a consequence of endocytosis,

disappearance as the sole criteria for endocytosis is insufficient because it is also observed when the clathrin coat disassembles during uncoating and as a result of photobleaching (Ehrlich et al., 2004; Merrifield et al., 2005; Mattheyses et al., 2011). Thus, a robust measure for CME requires demonstration of cargo internalization together with the disappearance of clathrin from the cell membrane, as seen in mammalian systems (Ehrlich et al., 2004; Merrifield et al., 2005; Rappoport et al., 2005; Mattheyses et al., 2011). Similar evidence of internalization of specific plasma membrane cargo via CME has been lacking in *Dictyostelium*. Furthermore, owing to the use of low temporal resolution and fixed-cell imaging for monitoring CME in *Dictyostelium*, there is limited dynamic information about the endocytosis of clathrin-coated vesicles.

In *Dictyostelium*, loss of expression of many different endocytic proteins results in a defect in osmoregulation, which is controlled by a specialized organelle called the contractile vacuole (Gerisch et al., 2002). Osmoregulation phenotypes of varying severity are observed in both clathrin light chain (*clc-*) (Wang et al., 2003) and heavy chain (*chcA-*) knockouts (O'Halloran and Anderson, 1992), as well as in knockouts of AP180 (Stavrou and O'Halloran, 2006), the  $\alpha$ ,  $\beta$ 1/2 or  $\mu$ 2 subunits of AP2 (Wen et al., 2009; Sosa et al., 2012), and the  $\mu$ 1 subunit of AP1 (Lefkir et al., 2003). Although the function of clathrin and its adaptors at the contractile vacuole is unclear, mislocalization of contractile vacuole components in AP1 and AP2 knockouts has suggested roles for these complexes in contractile vacuole biogenesis (Lefkir et al., 2003; Sosa et al., 2012).

To study CME vesicles in live cells, we identified a cargo protein and determined the members of the AP2 complex in *Dictyostelium*. Using biochemical and optical tools, we found that cargo, clathrin and AP2 in *Dictyostelium* have dynamics characteristic of endocytosis. The AP2 complex colocalizes with clathrin in plasma membrane puncta that internalize from the cell surface into the cytosol. Our results provide direct evidence for the existence of a clathrin-mediated pathway for endocytosis in *Dictyostelium*, detailed characterization of the kinetics of clathrin and AP2-containing vesicles, and establish a role for this pathway in the biogenesis of the contractile vacuole.

## Results

### Cloning and characterization of the *Dictyostelium* AP2 complex

Genes corresponding to the subunits of AP1, AP2, AP3 and AP4 in *Dictyostelium* were inferred from homology to their mammalian counterparts (supplementary material Table S1).

Experimental evidence has confirmed these annotations for the  $\gamma$ ,  $\beta$ 1/2 and  $\mu$ 1 subunits of AP1 (Lefkir et al., 2003), for the  $\delta$ ,  $\beta$ 3 and  $\mu$ 3 subunits of AP3 (Bennett et al., 2008) and for the  $\beta$ 1/2 and  $\mu$ 2 subunits of AP2 (Sosa et al., 2012). To investigate the AP2 complex in *Dictyostelium*, we cloned the *Ap2A1* gene and labeled it with green fluorescent protein (GFP) at the N terminus (GFP-Ap2A1). Expression of GFP-Ap2A1 in wild-type cells (AX2) resulted in the expression of a single 140-kDa protein, in agreement with the predicted size for GFP-Ap2A1 (Fig. 1A). Expression of this protein showed no detectable effect on doubling time or time taken by cells to undergo development (growth curves; development on agar; data not shown). To identify proteins that interact with GFP-Ap2A1 and form the AP2 complex, cells expressing GFP-Ap2A1 were lysed and incubated with an anti-GFP antibody. The co-immunoprecipitated proteins were separated by SDS-PAGE and the proteins identified by mass spectrometry. The proteins included the predicted  $\alpha$ ,  $\beta$ ,  $\mu$  and  $\sigma$  subunits of the AP2 complex (Fig. 1B; supplementary material Table S2). We identified the protein product of the gene *Ap1B1* as the  $\beta$  subunit, independently confirming the recent report that AP1 and AP2 use the same  $\beta$  subunit in *Dictyostelium* (Sosa et al., 2012). We also identified the protein products of the *apm2* gene as the  $\mu$ 2 subunit and of the *Ap2S1* gene as the  $\sigma$ 2 subunit; other AP complex subunits were not identified. We also identified the *Dictyostelium* homolog of Eps15, a clathrin adaptor known to bind to the AP2  $\alpha$  subunit in mammalian cells (van Delft et al., 1997). These results demonstrate the existence of a functional AP2 complex in *Dictyostelium* that is homologous to the AP2 complex found in mammals. Additionally, GFP-Ap2A1 was incorporated into this AP2 complex and, at the level of expression used here, did not localize to any other protein complexes in the cell.

### Intracellular localization and dynamics of clathrin and AP2 in *Dictyostelium*

Using GFP-Ap2A1 as a reporter for the AP2 complex, we investigated its localization within the cell. Confocal microscopy showed that GFP-Ap2A1 localized to distinct puncta that were distributed around the cell periphery (Fig. 2A), in agreement with a previous study that used antibodies raised against Ap2A1 (Wen et al., 2009). Imaging of cells by total internal reflection fluorescence microscopy (TIR-FM), which excites molecules within  $\sim$ 100 nm of the coverslip, enabled us to establish that AP2 puncta are at, or close to, the plasma membrane (Fig. 2B). TIR-FM time-lapse imaging of GFP-Ap2A1 revealed the dynamic nature of AP2 puncta: puncta appeared at the

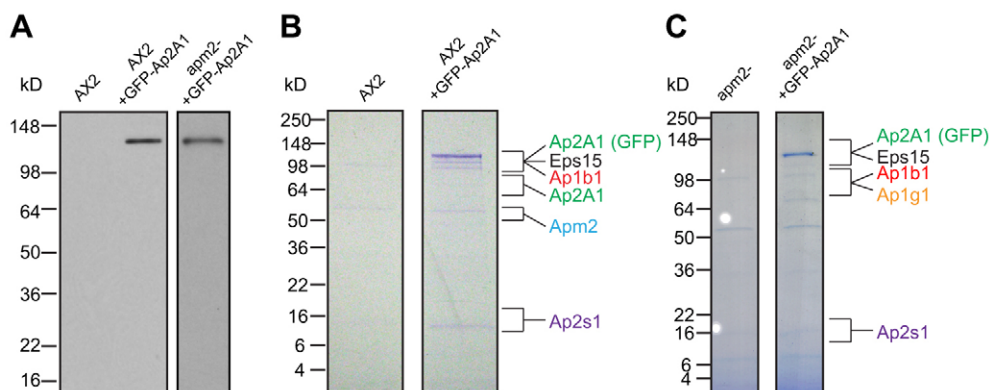


**Fig. 1. Molecular characterization of the AP2 complex.** (A) Western blot for GFP in lysates from wild-type cells (AX2) and GFP-expressing wild-type and *apm2-* cells. (B,C) Coomassie-stained SDS-PAGE gel of proteins immunoprecipitated with anti-GFP antibodies from (B) AX2, as well as AX2 expressing GFP-Ap2A1 and (C) *apm2-* and *apm2-* cells expressing GFP-Ap2A1. A list of all proteins uniquely identified by LC-MS/MS is in supplementary material Table S2.

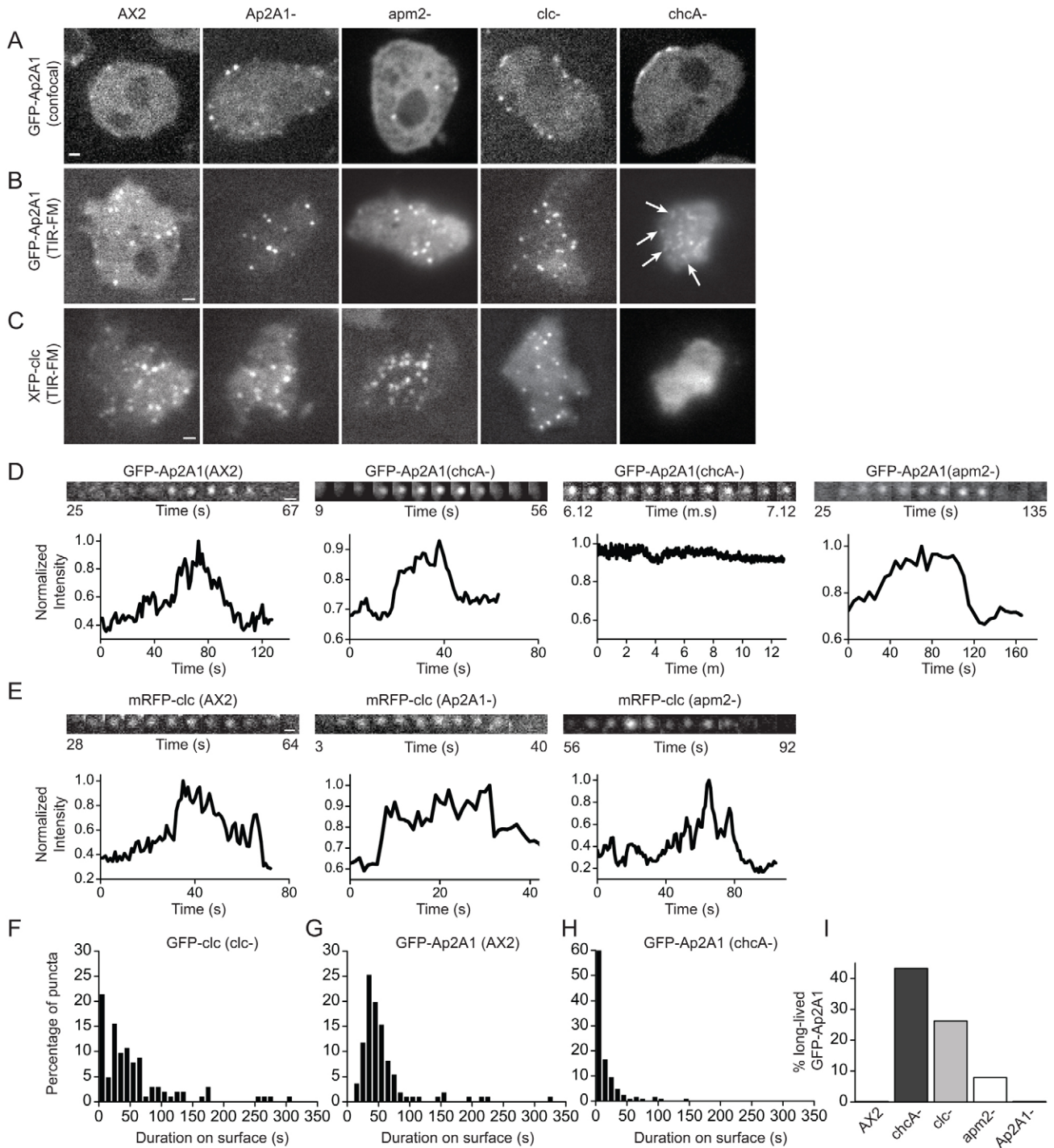


**Fig. 2. Intracellular localization and dynamics of clathrin and AP2.** (A) Confocal sections showing the intracellular localization of GFP-Ap2A1 in wild-type (AX2), *Ap2A1*<sup>-</sup>, *apm2*<sup>-</sup>, *clc*<sup>-</sup> and *chcA*<sup>-</sup> cells. (B) TIR-FM images of GFP-Ap2A1 puncta in AX2, *Ap2A1*<sup>-</sup>, *apm2*<sup>-</sup>, *clc*<sup>-</sup> and *chcA*<sup>-</sup> cells. (C) TIR-FM images of mRFP-clc puncta in AX2, *Ap2A1*<sup>-</sup>, *apm2*<sup>-</sup> and GFP-clc puncta in *clc*<sup>-</sup> cells. (D) Examples of the dynamics of individual GFP-Ap2A1 puncta imaged by TIR-FM in AX2, *chcA*<sup>-</sup> and *apm2*<sup>-</sup> cells. Normalized fluorescence intensity is plotted as a function of time for each punctum. (E) Examples of the dynamics of individual mRFP-clc puncta imaged by TIR-FM in AX2, *Ap2A1*<sup>-</sup> and *apm2*<sup>-</sup> cells. Normalized fluorescence intensity is plotted as a function of time for each punctum. (F–H) Cell surface duration of (F) GFP-clc puncta in *clc*<sup>-</sup> cells; (G) GFP-Ap2A1 puncta in AX2 cells; and (H) GFP-Ap2A1 in *chcA*<sup>-</sup> cells. (I) Percentage of GFP-Ap2A1 puncta present at the end of the time-lapse with durations >350 seconds. Scale bars: 1  $\mu$ m (A–C); 0.5  $\mu$ m (D,E). See also supplementary material Fig. S1 and Table S3.

membrane, remained there for various lengths of time and then disappeared from the TIR-FM field (Fig. 2D). Occasionally, AP2 puncta could be seen to localize in rings or circles

(supplementary material Fig. S1A), closely resembling AP2 puncta localization on bladders of the contractile vacuole (Wen et al., 2009) and, thus, were excluded from further analysis.

When AP2 puncta were imaged continuously for 7.5 seconds, three different puncta behaviors were observed:  $78 \pm 8\%$  remained static,  $16 \pm 8\%$  disappeared and  $7 \pm 5\%$  moved laterally (mean  $\pm$  s.d.;  $n=363$ ). When AP2 puncta were followed over a longer time period (time-lapse for 10 minutes), all the puncta observed to appear on the surface disappeared within 6 minutes, with an average duration on the surface of  $56.3 \pm 4.2$  seconds (mean  $\pm$  s.e.m.;  $n=111$ ) (Fig. 2G). Some puncta were lost owing to the movement of cells during the course of imaging and could not be included in the kinetic analysis. In an attempt to remove any potential bias in our manual tracking, we tested the use of automated tracking to follow every punctum in the cell. This method gave large errors and a significantly shorter duration because it did not exclude puncta that disappeared owing to cell movement. Thus, because of their highly motile nature, automated tracking is not a suitable approach to analyze the kinetics of endocytic puncta in *Dictyostelium*.

To compare the behavior of AP2 with clathrin, we imaged clathrin light chain-knockout cells (*clc-*) expressing GFP-tagged clathrin light chain (GFP-clc) (Wen et al., 2009) and performed the same analysis. In TIR-FM, GFP-clc localized to distinct membrane puncta as well as to contractile vacuoles, as previously observed (Fig. 2C; supplementary material Fig. S1A) (Brady et al., 2010; Wen et al., 2009). Continuous imaging of clathrin puncta for a 7.5-second period revealed their dynamic behavior, with  $55 \pm 18\%$  remaining static,  $26 \pm 14\%$  disappearing and  $19 \pm 5\%$  moving laterally (mean  $\pm$  s.d.;  $n=300$ ). When clathrin puncta were imaged over for a longer time period (time-lapse for 10 minutes), all puncta observed appearing on the surface disappeared within 5 minutes, with an average duration on the surface of  $55.6 \pm 6.0$  seconds (mean  $\pm$  s.e.m.;  $n=103$ ) (Fig. 2F). This is similar to the value of 39 seconds previously reported (Brady et al., 2010).

Comparison of clathrin and AP2 puncta showed that they had similar distributions of duration times at the cell surface (Fig. 2F,G); however, more clathrin puncta had shorter durations at the cell surface (21% of clathrin puncta have a lifetime  $<10$  seconds versus 0% of AP2 puncta). We believe that this population corresponds to clathrin-coated intracellular vesicles that move close to the plasma membrane during imaging, thus being detected using TIR-FM (Keyel et al., 2004). Using a two-sample Kolmogorov–Smirnov (KS) test, we saw that, if the puncta with durations  $<10$  seconds were removed from the clathrin population, the distribution of duration times was no longer significantly different between AP2 and clathrin (KS test,  $P=0.066$ ) (supplementary material Table S3).

The localization of clathrin in dynamic membrane puncta at the cell membrane was consistent with results from mammalian cells and showed that, in *Dictyostelium*, clathrin-coated pits form on the plasma membrane. Our results also showed that, in *Dictyostelium*, the localization and dynamics of AP2 are similar to those in mammalian cells and, therefore, AP2 puncta correspond to clathrin-coated pits.

### Clathrin heavy chain is required for the dynamic behavior of AP2 puncta

The formation and maturation of a clathrin-coated pit involves the recruitment of a complex array of proteins. It has been difficult to study the requirements for individual components of the clathrin-coated vesicle cycle in mammalian cells because of

redundancy and incomplete knockdowns. We took advantage of the availability of clathrin and AP2 knockouts in *Dictyostelium* to investigate whether they are required for the observed cell surface dynamics of puncta.

We expressed GFP-Ap2A1 in cells with either disrupted clathrin light chain (*clc-*) (Wang et al., 2003) or disrupted clathrin heavy chain (*chcA-*) (Ruscetti et al., 1994). TIR-FM imaging of GFP-Ap2A1 in *clc-* cells showed that AP2 was able to localize to membrane puncta that behaved with similar dynamics to wild-type cells (Fig. 2A,B; supplementary material Fig. S1C,E).

In *chcA-* cells, although GFP-Ap2A1 was able to form membrane puncta with a normal appearance, there was an increased number of diffuse puncta compared with wild-type cells (Fig. 2B). In addition, there was cell-to-cell variability, with some cells showing no puncta. We analyzed AP2 puncta by fitting a single-peak two-dimensional (2D) Gaussian curve to individual puncta, the width of the Gaussian where it falls to  $1/e$  of the maximum was then measured for each punctum. The average width of AP2 puncta in *chcA-* cells was  $3.7 \pm 1.8$  pixels (mean  $\pm$  s.d.;  $n=391$ ) compared with  $2.9 \pm 0.8$  pixels in wild-type cells ( $n=461$ ); this difference was statistically significant (*t*-test,  $P \leq 0.001$ ). Confocal imaging of GFP-Ap2A1 in *chcA-* cells showed that, although GFP-Ap2A1 could bind to the membrane, the puncta often stuck together and localized to one side of the cell (Fig. 2A). Furthermore, time-lapse TIR-FM imaging showed high variability in the behavior of individual AP2 puncta; several puncta were very short lived (durations  $<10$  seconds), some had dynamics indistinguishable from the wild type, whereas others were long lived (present at the beginning of imaging and did not disappear for over a 12-minute period) (Fig. 2D). Analysis of the time for which the dynamic GFP-Ap2A1 puncta were detectable on the surface showed an increased proportion of puncta with durations of  $<10$  seconds, causing a significantly shorter average surface duration of  $15.2 \pm 2.0$  seconds (mean  $\pm$  s.e.m.;  $n=127$ ) compared with wild-type cells ( $52.3 \pm 4.2$  seconds) (Fig. 2H); correspondingly, the distribution of durations was significantly different between wild-type and *chcA-* cells (KS test,  $P=3.80 \times 10^{-32}$ ). To analyze the long-lived puncta, we quantified the time of arrival of puncta present at the end of the time-lapse to determine how many had a duration greater than 350 seconds. For wild-type cells, we did not observe any puncta with a duration  $>350$  seconds; however, in *chcA-* cells, we found that 43.3% of the GFP-Ap2A1 puncta had a duration  $>350$  seconds. This number was also elevated in *clc-* cells (26.3%) (Fig. 2I). This shows that, although clathrin is not required for the plasma membrane localization of AP2, its loss results in the appearance of two abnormal AP2 puncta populations, one that is very short lived and one that is long lived. This suggests that clathrin has roles in both stabilizing AP2 binding at the membrane and the progression of AP2 puncta to internalization.

### AP2 $\mu 2$ is not required for AP2 $\alpha$ puncta formation

We next investigated the effects of disrupting the  $\alpha$  (*Ap2A1-*) (Wen et al., 2009) or  $\mu 2$  (*apm2-*) (Mercanti et al., 2006b) subunits on the localization and dynamics of AP2 or clathrin in cells (Fig. 2B,C). In both the  $\alpha$  and  $\mu 2$  knockouts, clathrin puncta at the plasma membrane were similar to wild-type cells (Fig. 2C,E; supplementary material Fig. S1B,G; Table S3). TIR-FM imaging of GFP-Ap2A1 in *Ap2A1-* cells showed some

puncta with dynamics in the range of wild-type cells; however, the distribution of durations was significantly different (KS test,  $P=0.0094$ ) because of the appearance of a population with shorter durations ( $<20$  seconds) (supplementary material Fig. S1C,E; Table S3). This could be because of an incomplete rescue of the *Ap2A1*<sup>-</sup> phenotype by the GFP-*Ap2A1* protein. Interestingly, in  $\mu 2$  knockouts, GFP-*Ap2A1* also localized to distinct membrane puncta, some of which behaved with dynamics in the range of wild-type cells. A population with shorter durations also appeared, making the distributions significantly different (KS test,  $P=2.23 \times 10^{-5}$ ) (Fig. 2B,D; supplementary material Fig. S1C,E; Table S3). Confocal imaging showed that, although GFP-*Ap2A1* puncta could be seen on the plasma membrane in *apm2*<sup>-</sup> cells, there was a higher cytoplasmic level of GFP-*Ap2A1* (Fig. 2A). Western blot of cell lysates showed that loss of  $\mu 2$  does not destabilize the  $\alpha$  subunit (Fig. 1A), consistent with the finding that the  $\beta 1/2$  subunit is also stable in *apm2*<sup>-</sup> cells (Sosa et al., 2012). To investigate the composition of the GFP-*Ap2A1* puncta, we incubated lysates from *apm2*<sup>-</sup> cells expressing GFP-*Ap2A1* with an anti-GFP antibody and separated and identified the co-immunoprecipitated proteins using SDS-PAGE and mass spectrometry (Fig. 1C). We found that, in the absence of the  $\mu 2$  subunit, GFP-*Ap2A1* was still able to interact with the  $\beta 1/2$  (*Ap1B1*) and  $\sigma 2$  (*Ap2S1*) subunits of the AP2 complex. Although we did not find any of the other AP  $\mu$  subunits, we did identify the  $\gamma$  subunit of AP1 (*Ap1G1*). These results indicate that, in the absence of the  $\mu 2$  subunit in *Dictyostelium*, a partial AP2 complex can form that contains the  $\gamma$  subunit.

### Clathrin and AP2 puncta colocalize and disappear together

To test the hypothesis that clathrin and AP2 puncta corresponded to clathrin-coated pits, we investigated their behavior in the same

cell. Both mRFP-*clc* and GFP-*Ap2A1* colocalized in puncta at the plasma membrane in live cells, in agreement with observations in fixed cells (Fig. 3A) (Wen et al., 2009). Colocalization analysis demonstrated that  $76 \pm 18\%$  of AP2 puncta were positive for clathrin and  $57 \pm 19\%$  of clathrin puncta were positive for AP2 (mean  $\pm$  s.d.;  $n=33$  cells) (Fig. 3C). Colocalization of less than 100% is consistent with observations of clathrin and AP2 in mammalian cells (Rappoport et al., 2003).

Two color TIR-FM time-lapse imaging of puncta showed that GFP-*Ap2A1* and mRFP-*clc* displayed similar dynamics at the plasma membrane (Fig. 3B,D). Individual puncta were analyzed by calculating the time of disappearance from the TIR field for both GFP-*Ap2A1* and mRFP-*clc* ( $n=132$ ) (Fig. 3E). This analysis showed that, for 58% of puncta, AP2 disappeared within 4 seconds of clathrin disappearance; thus, we conclude that AP2 and clathrin leave the TIR field at similar times and behave with similar dynamics at the plasma membrane.

### Clathrin and AP2 disappearance corresponds to endocytosis

To further investigate the nature of AP2 and clathrin disappearance, we monitored these puncta by alternating between widefield (EPI) and TIR. Given that the TIR field decays with a space constant of  $\sim 100$  nm but the EPI field has a focal depth of  $\sim 500$  nm, puncta that are internalized should continue to be detected with EPI illumination after disappearing from the TIR field (Merrifield et al., 2002; Matheyses et al., 2011).

Cells expressing GFP-*Ap2A1* and *clc*-mRFP were imaged by alternating EPI and TIR illumination and the fluorescence intensity of individual puncta was quantified for each channel and used to group puncta based on their behavior (Fig. 4). Puncta

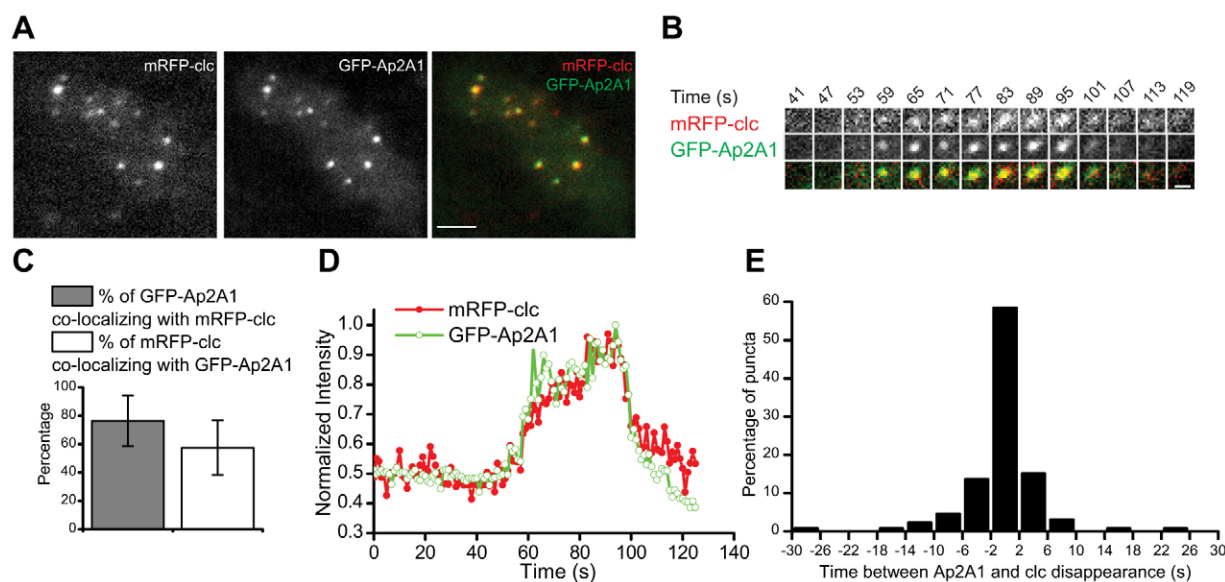


**Fig. 3. Simultaneous imaging of the dynamics of clathrin and AP2.** (A) Two-color TIR-FM images of GFP-*Ap2A1* and mRFP-*clc* puncta. Scale bar: 2  $\mu$ m. (B) Example of dynamics of an individual punctum imaged by TIR-FM. Scale bar: 0.5  $\mu$ m. (C) Quantification of colocalization between GFP-*Ap2A1* and mRFP-*clc* puncta imaged by TIR-FM. The percentage overlap is plotted for GFP-*Ap2A1* versus mRFP-*clc* (gray bar) and for mRFP-*clc* versus GFP-*Ap2A1* (white bar). Data are represented as mean  $\pm$  s.d. ( $n=33$  cells). (D) Normalized fluorescence intensity for the punctum shown in B is plotted as a function of time for GFP-*Ap2A1* (green, open circles) and mRFP-*clc* (red, filled circles). (E) Time between mRFP-*clc* and GFP-*Ap2A1* disappearance from the TIR-FM field ( $n=132$  puncta).

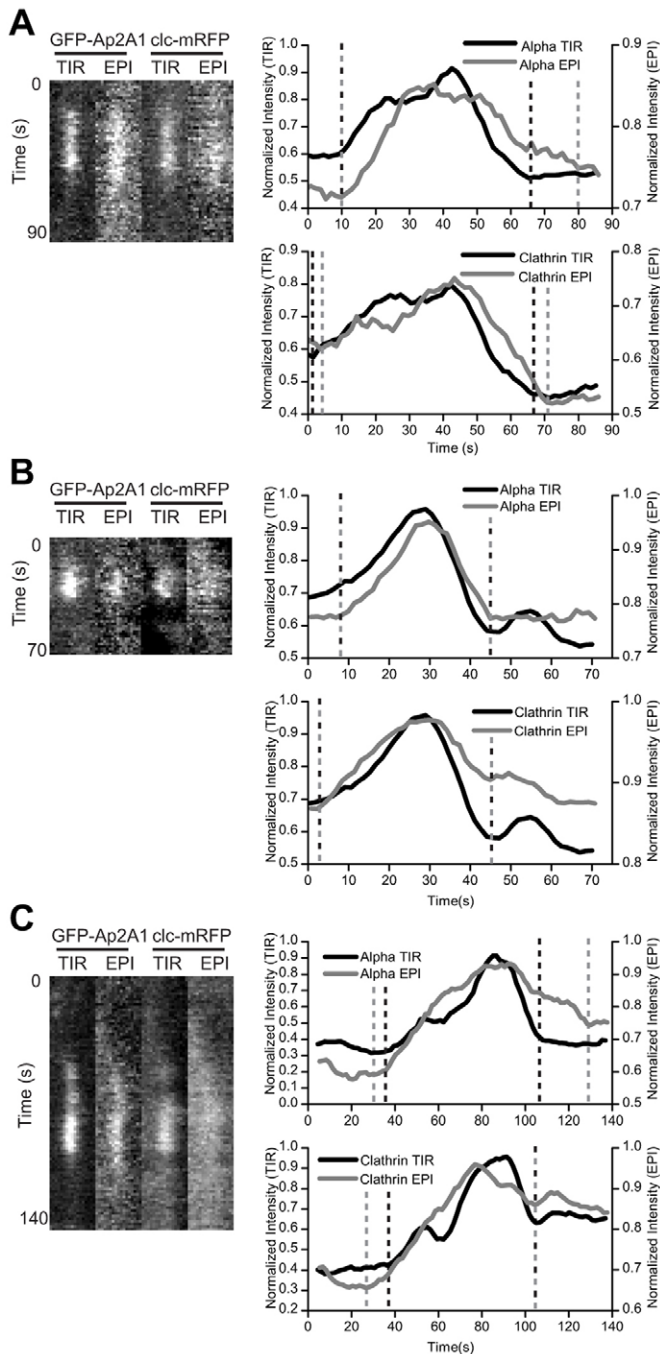


**Fig. 4. Identification of internalizing puncta.** Examples of the dynamics of individual GFP-Ap2A1 and clc-mRFP puncta imaged by two-color alternating EPI and TIR illumination. Kymographs are a maximum intensity projection of the four pixels surrounding the center of the punctum. Normalized fluorescence intensity is plotted as a function of time for GFP-Ap2A1 TIR signal (top graph, black line), GFP-Ap2A1 EPI signal (top graph, gray line), clc-mRFP TIR signal (bottom graph, black line) and clc-mRFP EPI signal (bottom graph, gray line). Lines indicate the time of either appearance or disappearance for each channel. (A) An individual punctum where the EPI and TIR signals appear together and the TIR signal disappears before the EPI signal. (B) An individual punctum where the EPI and TIR signals appear and disappear together. (C) An individual punctum where the EPI signal appears before the TIR signal.

were only analyzed if, by TIR, they could be seen in both the GFP (AP2) and RFP (clathrin) channels, and the fluorescence signal accumulated in a punctum followed by a rapid disappearance from TIR. For some puncta, the clathrin EPI signal could not be detected above the noise; in these cases, only the AP2 EPI signal was used for analysis. A vesicle that formed in TIR, pinched off the membrane and moved into the cell, consistent with endocytosis, was observed for  $32 \pm 17\%$  of puncta (mean  $\pm$  s.d.;  $n=93$ ) (Fig. 4A). For these puncta, the fluorescence appeared in EPI simultaneously with, or soon after, the TIR signal, consistent with the *de novo* formation of a clathrin-coated pit at the plasma membrane, and inconsistent with an internal vesicle moving towards the cell surface. When these puncta subsequently disappeared from the TIR field, they continued to be observed in EPI illumination, indicating movement away from the plasma membrane into the cell.

For  $17 \pm 13\%$  of puncta, the EPI signal appeared and disappeared simultaneously with the signal in TIR (Fig. 4B). These events could correspond to endocytic vesicles that either lose their clathrin and AP2 coincident with the vesicle leaving the plasma membrane, or to vesicles internalizing faster than the imaging speed. Alternatively, the loss of signal could be because of an unproductive clathrin-coated pit where clathrin and AP2 disassemble at the cell membrane. Both of these behaviors have been reported in mammalian cells (Mattheyses et al., 2011). A small percentage ( $12 \pm 6\%$ ) of puncta had an EPI signal that appeared before the TIR signal and, thus, appeared to be internal vesicles that entered the TIR field (Fig. 4C) and not clathrin-coated vesicles formed *de novo*. In  $39 \pm 18\%$  of puncta, the EPI signal was not bright enough to distinguish from the background fluorescence in the cytoplasm, hence their fate could not be classified. We expect that the behavior of these puncta will be equally distributed between the behaviors observed above and so conclude that most ( $>50\%$ ) AP2 and clathrin puncta that disappeared from the TIR field showed behavior that corresponded to productive endocytic events.

#### Dajumin-GFP is a plasma membrane cargo for clathrin-mediated endocytosis

Given that clathrin and AP2 have a role in osmoregulation in *Dictyostelium* (Wen et al., 2009; O'Halloran and Anderson, 1992), we examined whether CME is involved in retrieval of the contractile vacuole proteins that might have entered the cell membrane. Although contractile vacuoles are thought to fuse with the plasma membrane by a kiss-and-run mechanism that does not involve any membrane mixing (Heuser, 2006; Gabriel et al., 1999), it is possible that there is a low level of leakage into the plasma membrane upon pore formation (Wen et al., 2009; Gabriel et al., 1999; Sosa et al., 2012).

We coexpressed the contractile vacuole specific marker protein dajumin-GFP (Gabriel et al., 1999) with mRFP-clc and imaged cells with TIR-FM (Fig. 5A). Dajumin-GFP labeling of the contractile vacuole could be seen as bright bladders and tubules close to the basal membrane, as described previously (Gabriel et al., 1999). Closer inspection of our images revealed that dajumin-GFP also localized to dim puncta that colocalized with mRFP-clc puncta (Fig. 5A). Colocalization analysis showed that  $40 \pm 14\%$  of mRFP-clc overlapped with dajumin-GFP and  $22 \pm 12\%$  of dajumin-GFP overlapped with mRFP-clc (mean  $\pm$  s.d.;  $n=25$  cells) (Fig. 5B). Colocalization was validated by performing a pixel shift analysis showing that the peak

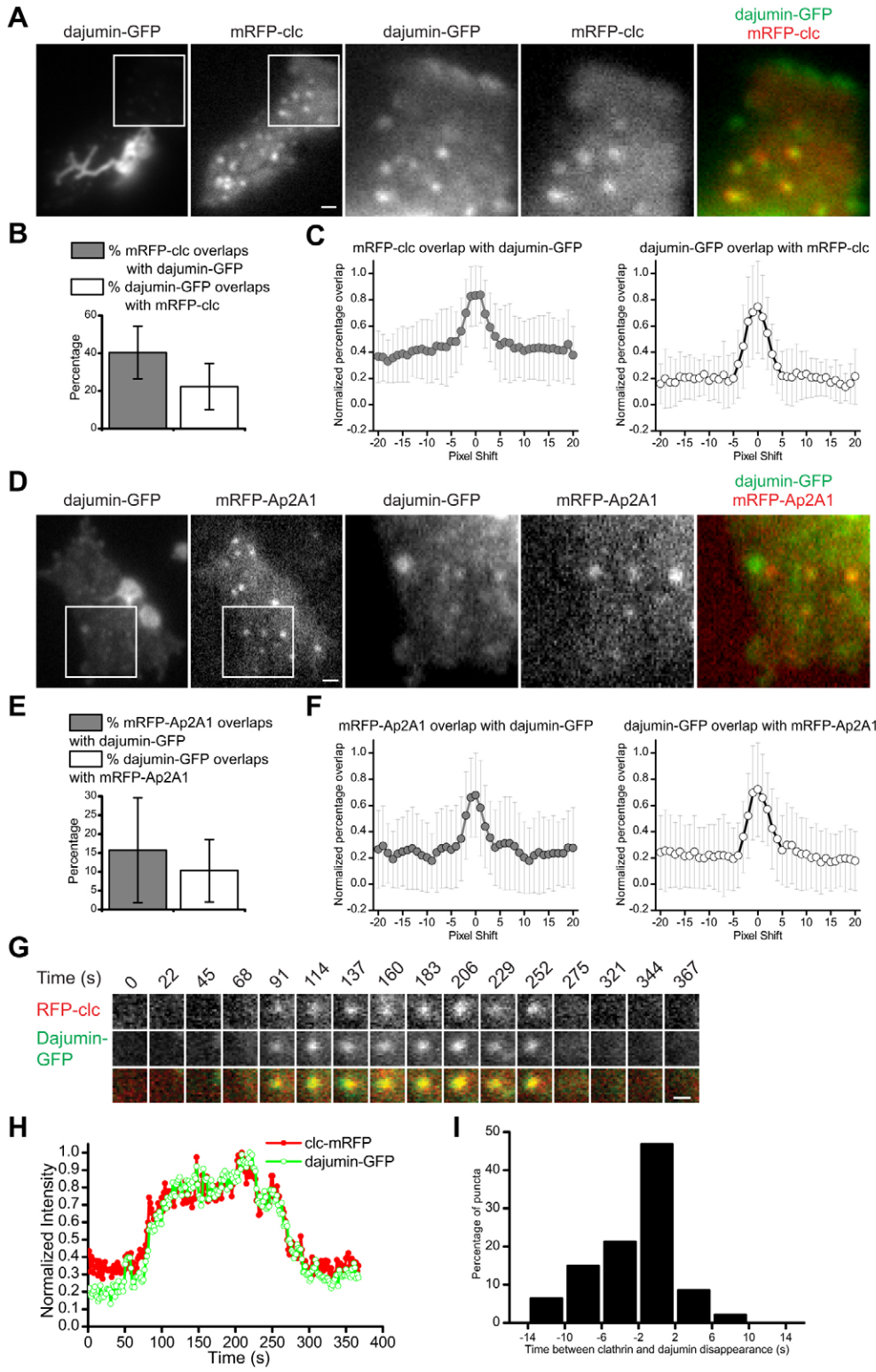


**Fig. 5. Simultaneous imaging of the dynamics of clathrin and dajumin-GFP.** (A,D) Two-color TIR-FM images of dajumin-GFP and mRFP-clc (A) or dajumin-GFP and mRFP-Ap2A1 (D). The enlarged images enable visualization of dajumin-GFP puncta; intensities are rescaled. Scale bar: 1  $\mu$ m. (B,E) Quantification of colocalization between dajumin-GFP and mRFP-clc (B) or between dajumin-GFP and mRFP-Ap2A1 (E). Data are represented as mean  $\pm$  s.d. [(B)  $n=25$  cells, (E)  $n=45$  cells]. (C,F) Pixel shift analysis of colocalization was performed on each cell. The graph shows the percentage overlap as a function of shifting the images one pixel to the left (negative numbers) or right (positive numbers). Data are represented as mean normalized percentage overlap  $\pm$  s.d. (G) Dynamics of an individual dajumin-GFP and mRFP-clc punctum imaged by TIR-FM. Scale bar: 0.5  $\mu$ m. (H) Normalized fluorescence intensity for the punctum shown in G is plotted as a function of time for dajumin-GFP (green, open circles) and mRFP-clc (red, filled circles). (I) Time between mRFP-clc and dajumin-GFP disappearance from the TIR-FM field ( $n=47$  puncta).

colocalization overlap was in the nonshifted image ( $dx=0$ ) (Fig. 5C). Colocalization quantification was confounded by the relatively dim fluorescence of dajumin-GFP puncta; they appeared and disappeared and were not present at each time point. As a result, there was considerable cell-to-cell variability in the percentage overlap.

In cells expressing Ap2A1 tagged with mRFPmars (mRFP-Ap2A1) and dajumin-GFP (Fig. 5D), we found, by TIR-FM, dajumin-GFP puncta that colocalized with mRFP-Ap2A1. Colocalization analysis showed  $16 \pm 14\%$  of mRFP-Ap2A1 overlapped with dajumin-GFP and  $10 \pm 8\%$  of dajumin-GFP overlapped with mRFP-Ap2A1 (mean  $\pm$  s.d.;  $n=45$  cells)

(Fig. 5E). Again, there was cell-to-cell variability and colocalization was validated using pixel shift analysis (Fig. 5F). The colocalization of this transmembrane protein with AP2 and clathrin suggested that it was internalized in clathrin-coated vesicles.

To investigate the dynamics of dajumin-GFP puncta, we used time-lapse imaging of cells expressing dajumin-GFP and mRFP-clc (Fig. 5G). Puncta were tracked over time and the fluorescence intensity was quantified (Fig. 5H). Dajumin-GFP accumulated with clathrin followed by a rapid disappearance from the TIR field. The time of initiation of disappearance from the TIR field was calculated for both dajumin-GFP and mRFP-clc for each

punctum ( $n=47$ ) (Fig. 5I). This analysis showed that 47% of dajumin-GFP puncta disappeared together with clathrin ( $<4$  seconds apart). Given that we showed that clathrin puncta that disappeared from TIR moved into the cell (Fig. 4), we conclude that dajumin-GFP is internalized from the plasma membrane of *Dictyostelium* via CME.

### Clathrin heavy chain is essential for internalization of plasma membrane dajumin-GFP

Internalization of dajumin-GFP from the plasma membrane was confirmed using a biotin internalization assay (Barth et al., 1994) (Fig. 6A). Plasma membrane proteins of wild-type cells

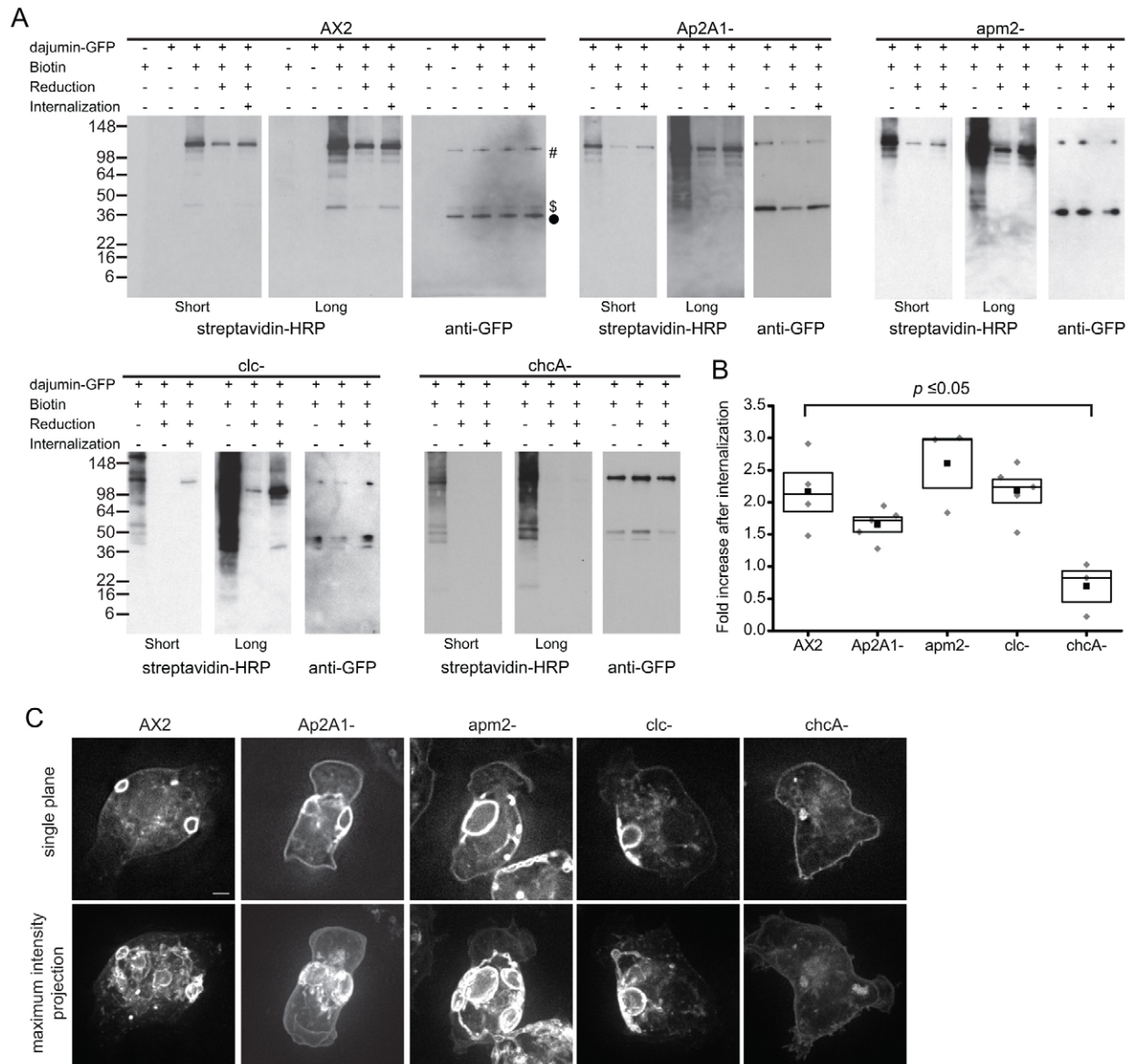


**Fig. 6. Internalization of dajumin-GFP.** (A) Biotin internalization assay for AX2, *Ap2A1*<sup>-</sup>, *apm2*<sup>-</sup>, *clc*<sup>-</sup> and *chcA*<sup>-</sup> cells. Dajumin-GFP was immunoprecipitated from cell lysates. Membranes were probed for biotin with streptavidin-HRP (short and long exposures shown) or for GFP with an anti-GFP antibody. Dajumin-GFP full-length protein (#), the 45-kDa fragment (\$) and the 40-kDa fragment (•) are indicated. (B) The -fold increase in biotin signal following 15 minutes of internalization calculated from western blots. Solid square, mean; box, s.e.m. and 50th percentile; gray diamond, individual values. Values were compared using a one-way ANOVA. (C) Widefield microscopy images of dajumin-GFP in AX2, *Ap2A1*<sup>-</sup>, *apm2*<sup>-</sup>, *clc*<sup>-</sup> and *chcA*<sup>-</sup> cells. A single focal plane (top row) and a maximum intensity projection of the entire cell (bottom row) are shown. Scale bar: 1  $\mu$ m. See also supplementary material Fig. S2.

expressing dajumin-GFP were reversibly biotinylated with a membrane-impermeable biotin. Immunoprecipitation of dajumin-GFP from cell lysates, followed by SDS-PAGE and western blot analysis with streptavidin-HRP, showed that dajumin-GFP is biotinylated and, thus, present on the plasma membrane. Western blot analysis of dajumin-GFP showed that the full-length protein and two cleavage products (45 kDa and 40 kDa) were present in cells (Gabriel et al., 1999). Tagging of dajumin on its extracellular domain confirmed that these are products of cleavage and indicated the protein is cleaved at, or close to, the transmembrane domain (data not shown). Only the full-length protein and the 45-kDa fragment were biotinylated; the 40-kDa fragment was either not on the plasma membrane or did not have extracellular amino groups accessible to the biotinylation reagent.

We next followed the fate of cell surface dajumin-GFP by allowing the cells to internalize proteins for 15 minutes by incubation at 22°C. Residual cell surface biotin was removed by incubation with a membrane-impermeable reducing agent. As a control, some cells were kept on ice and, thus, did not undergo any cell surface internalization. The results show that following the internalization step at 22°C, the amount of biotinylated dajumin-GFP increased, demonstrating endocytosis from the cell surface.

We assessed the requirement of clathrin and AP2 for internalization by expressing dajumin-GFP in *Ap2A1*<sup>-</sup>, *apm2*<sup>-</sup>, *clc*<sup>-</sup> and *chcA*<sup>-</sup> cells. In *Ap2A1*<sup>-</sup>, *apm2*<sup>-</sup> and *clc*<sup>-</sup> cells, the amount of biotinylated dajumin-GFP increased following the internalization step, showing that plasma membrane dajumin-GFP was internalized similar to wild-type cells. By contrast, in *chcA*<sup>-</sup> cells, dajumin-GFP was biotinylated and, therefore, was on the plasma membrane, but no internalization was ever observed (Fig. 6A,B).

We confirmed these results by imaging the localization of dajumin-GFP in the various cell lines (Fig. 6C). In wild-type, *Ap2A1*<sup>-</sup>, *apm2*<sup>-</sup> and *clc*<sup>-</sup> cells, deconvolution of z-stacks showed the predominant localization of dajumin-GFP to be in contractile vacuoles, in agreement with recently published results (Sosa et al., 2012). The additional plasma membrane localization of dajumin-GFP that can be seen in individual focal planes has, however, not previously been described. In *chcA*<sup>-</sup> cells, no contractile vacuoles were observed (O'Halloran and Anderson, 1992) and dajumin-GFP was predominantly localized to the plasma membrane (Fig. 6B), again in agreement with (Sosa et al., 2012). The absence of contractile vacuoles in *chcA*<sup>-</sup> cells was confirmed by staining with the lipophilic dye FM4-64 (Heuser et al., 1993) and with an antibody to the vacuolar proton pump (VatM) (Fok et al., 1993) (supplementary material Fig. S2). Some internal dajumin-GFP positive structures could be seen; these did not colocalize with a fluid-phase endocytic marker or a lysosomal marker (10 kDa TxR-dextran; LysoTracker DND Blue; data not shown) and might represent either a rudimentary contractile vacuole that has not fused with the plasma membrane or the dajumin-GFP transiting through the Golgi compartment.

Together, our results show the existence of a clathrin-mediated endocytic pathway via which plasma membrane dajumin-GFP is internalized in a clathrin-dependent, AP2-independent mechanism. This suggests that internalization from the plasma membrane by clathrin-coated vesicles is important for the biogenesis and maintenance of the contractile vacuole in *Dictyostelium*.

## Discussion

The formation of clathrin-coated vesicles is characterized by the successive binding of various proteins. The adaptor complex AP2

acts as a central player in this process by binding to clathrin, many other accessory proteins and cargo (McMahon and Boucrot, 2011). We showed that a heterotetrameric AP2 complex exists in *Dictyostelium* that localizes to internalizing clathrin-coated pits on the plasma membrane. Given that AP1 and AP2 use the same  $\beta$  subunit in *Dictyostelium* (Sosa et al., 2012), and the AP1 complex has been shown to localize to the Golgi (Lefkir et al., 2003), membrane specificity of the AP complexes is not conferred by the  $\beta$  subunit. This is consistent with studies of mammalian AP complexes, which showed that  $\beta$  subunits primarily have a role in clathrin binding rather than membrane specificity (Page and Robinson, 1995; Shih et al., 1995).

In *Dictyostelium*, clathrin and AP2 showed similar dynamics at the membrane and, when imaged simultaneously, they colocalized in puncta and disappeared from the TIR-FM field together. This signature is consistent with the behavior of AP2 and clathrin puncta in mammalian cells (Rappoport et al., 2006). For both AP2 and clathrin puncta, there was a variety of durations on the plasma membrane, again a property consistent with mammalian clathrin-coated pits (Mattheyses et al., 2011). We took advantage of the spatial selectivity of TIR-FM compared with wide-field illumination to image the internalization of clathrin-coated pits as they moved from the plasma membrane into the cell. Taken together, our results demonstrated that AP2 and clathrin accumulate at clathrin-coated pits that disappear from the TIR-FM field, corresponding to productive endocytic events in *Dictyostelium*.

Deletions in clathrin and AP2 genes in *Dictyostelium* were used to study the requirements for these proteins in clathrin-coated vesicle formation. Our results showed that AP2 can form membrane puncta in the absence of clathrin heavy chain but that some of these puncta cannot progress to internalization, similar to observations in mammalian cells (Henne et al., 2010). These results suggest that the progressive nature and precise timing of forming a clathrin-coated vesicle have been conserved throughout evolution. Furthermore, we also observed a population of AP2 puncta that has a much shorter surface duration, indicating that clathrin also has a role in stabilizing AP2 at the membrane.

In the absence of the AP2  $\mu$ 2 subunit, GFP-*Ap2A1* was stable and able to localize to plasma membrane puncta of partial AP2 complexes. This suggests that the AP2 complex can assemble and target to the plasma membrane without the  $\mu$ 2 subunit, consistent with findings for AP1 in *Dictyostelium* (Lefkir et al., 2003). It is possible that the AP complexes are more dynamic than previously thought, with subunits functioning independently or exchanging freely. Interestingly, we also detected the  $\gamma$  subunit of AP1 in our co-immunoprecipitation. Given that AP1 and AP2 use the same  $\beta$  subunit, it is possible that we detected the  $\gamma$  subunit via this interaction. The appearance of a short-lived population of AP2 puncta in the  $\mu$ 2 and  $\alpha$  knockouts suggested that the individual subunits have a role in stabilizing the binding of the AP2 complex to the membrane.

Given that clathrin mutants are not lethal in unicellular organisms, such as *Dictyostelium* and yeast (O'Halloran and Anderson, 1992; Payne and Schekman, 1985; Lemmon and Jones, 1987), it has been suggested that CME acts as a nonspecialized endocytic portal in these lower eukaryotes (McMahon and Boucrot, 2011). For the first time in *Dictyostelium*, we have shown that a specific transmembrane cargo, dajumin-GFP, is internalized via CME. Just as clathrin is

required for internalization of many cargos in mammalian cells, internalization of dajumin-GFP is fully dependent on clathrin. Interestingly, its uptake is not dependent on AP2 suggesting that, in *Dictyostelium*, AP2 is not essential to form clathrin-coated vesicles, a property normally associated with CME in mammalian cells (Motley et al., 2003; Henne et al., 2010; Boucrot et al., 2010). Endocytosis independent of AP2 function is also seen in yeast (Huang et al., 1999; Yeung et al., 1999); thus, dependence on AP2 might have arisen in metazoans. However, AP2 function might not have been fully removed in *apm2*-knockouts owing to the presence of a partial AP2 complex that is still able to localize properly. Selection of dajumin-GFP as cargo might depend on the adaptor AP180, which has already been shown to have a role in retrieving Vamp7B from contractile vacuoles, limiting their homotypic fusion (Wen et al., 2009).

A role for clathrin and AP1 in contractile vacuole biogenesis is well documented (O'Halloran and Anderson, 1992; Wang et al., 2003; Lefkir et al., 2003; Sosa et al., 2012). In AP1  $\mu$ 1-knockouts, the contractile vacuole is completely absent, and the contractile vacuole proteins Rh50 and dajumin-GFP are mislocalized to punctate structures inside the cell (Lefkir et al., 2003; Sosa et al., 2012), indicating that at least some contractile vacuole components are trafficked in a clathrin-coated vesicle dependent mechanism. Dajumin-GFP localization to the plasma membrane in *chcA*- and  $\beta$ 1/2-knockout cells was previously reported (Sosa et al., 2012); this study suggests that AP2 only functions in sorting of dajumin-GFP in the context of an AP1 knockout. In agreement, we found that there was no observed defect in dajumin-GFP trafficking in AP2 knockouts alone; however, we showed that dajumin-GFP traffics through the plasma membrane even in wild-type cells, suggesting that this pathway operates normally, and not only in the context of mis-sorting by a AP1 knockout.

Our data showed a role for CME in the biogenesis and/or maintenance of the contractile vacuole by functioning in retrieval of proteins from the cell membrane. This is in agreement with results for Rh50 showing that a fusion protein with the cytoplasmic tail of Rh50 traffics via the plasma membrane en route to the contractile vacuole (Mercanti et al., 2006a). It also suggests the plasma membrane is a potential source of membrane for the contractile vacuole. It is possible that CME arose as a mechanism of protein sorting and has evolved to serve other functions in higher eukaryotes. Further identification of cargoes internalized by CME in *Dictyostelium* will help in addressing whether it performs only a sorting function in this organism.

In addition to its biosynthetic route, dajumin-GFP might enter the plasma membrane upon emptying of the contractile vacuole. Membrane mixing and entry of dajumin-GFP to the plasma membrane is not observed upon kiss-and-run fusion pore formation (Heuser, 2006; Gabriel et al., 1999). However, CME might function as a back-up mechanism in case of membrane mixing. It is unclear whether CME has any role in the regulation of contractile vacuole emptying and pore formation itself.

Our results offer the first direct demonstration that clathrin is utilized for endocytosis of membrane cargo in *Dictyostelium* in a process distinct from macropinocytosis and phagocytosis. This pathway is distinguished by the generation of endocytic vesicles that contain AP2, clathrin and dajumin. Furthermore, our analysis of this pathway at a high spatial and temporal resolution shows the high degree of similarity in the kinetics of internalization of individual clathrin-coated vesicles between *Dictyostelium* and

mammalian cells. These similarities support the conclusion that the formation of clathrin-coated vesicles is homologous between *Dictyostelium* and mammals and that *Dictyostelium* is a useful model to study CME *in vivo*.

## Materials and Methods

### Plasmid construction

To generate mRFPmars-Ap2A1 (mRFP-Ap2A1), the coding region of *Ap2A1* was amplified from a cDNA library and inserted into the vector 339-3 (Fischer et al., 2004) (provided by Dr A. Müller-Taubenberger) to generate GFP-Ap2A1, mRFPmars was replaced with GFP. Either GFP-Ap2A1 or mRFP-Ap2A1 was inserted into plasmids pDM304, pDM326 and/or pDM358 (Veltman et al., 2009) to allow selection with other resistance markers.

To generate mRFPmars-clc (mRFP-clc), the clc sequence from pTX-GFP-clc (Wang et al., 2006) (provided by Dr T. O'Halloran) was inserted into 339-3, mRFP-clc was then inserted into pDM304 for expression. To generate clc-mRFPmars (clc-mRFP), first mRFPmars was inserted into pDM304 or pDM326 to generate pDM304-mRFP(C) and pDM326-mRFP(C). The clc sequence was then inserted into pDM304-mRFP(C) and pDM326-mRFP(C).

The plasmid encoding dajumin-GFP was provided by Dr A. Müller-Taubenberger (Gabriel et al., 1999). Dajumin was inserted into pDM326-mGFP(C) to generate dajumin-mGFP.

### Cell growth

AX2 cells were cultured axenically in HL5 medium at 22°C. The knockout cell lines used were *Ap2A1*-, *apm2*-, *clc*- and *chcA*- and were provided by the Dicty Stock Center ([www.dictybase.org](http://www.dictybase.org)). Expression constructs were introduced into cells by electroporation and selected and maintained in HL5 medium containing 20  $\mu$ g/ml Geneticin, 10  $\mu$ g/ml BlasticidinS or 35  $\mu$ g/ml Hygromycin. A table of expression constructs and strains can be found in the supplementary material Table S4.

### Western blots

Cells were lysed on ice with RIPA buffer containing protease inhibitors. SDS sample buffer was added to 16  $\mu$ g of protein and run on a 4–20% Tris-glycine gel followed by transfer to nitrocellulose membranes. Membranes were blocked with 5% nonfat milk in TBS-T and probed with anti-GFP antibody (Novus NB600-303; 1:2000 or Clontech JL-8; 1:5000) followed by anti-rabbit-HRP (Sigma A0545; 1:50,000) or anti-mouse-HRP (Sigma A9917; 1:5000). HRP was visualized using Supersignal West Pico Chemiluminescent Substrate (Pierce) or ECL Plus (GE).

### Co-immunoprecipitation assay

Growth phase cells ( $9 \times 10^7$ ) were collected at 600 g for 2 minutes and lysed on ice in 10 ml of lysis buffer (10 mM Tris-Cl pH 7.5, 150 mM NaCl, 0.5 mM EDTA, 0.5% NP-40) for 30 minutes with pipetting every 10 minutes. The lysate was cleared by centrifugation at 20,000 g for 10 minutes at 4°C and the supernatant was collected. 60  $\mu$ l of GFP-Trap-A beads (ChromoTek) was washed in dilution buffer (10 mM Tris-Cl pH 7.5, 150 mM NaCl, 0.5 mM EDTA) according to the manufacturer's instructions and then added to the cell lysate and nutated for 5 hours at 4°C. Beads were collected by centrifugation at 2,000 g and washed with 1 ml of dilution buffer followed by a wash with 1 ml of dilution buffer containing 0.5 M NaCl. Proteins were eluted from the beads by adding 50  $\mu$ l of 2X SDS sample buffer followed by boiling for 10 minutes. Beads were collected at 2,700 g and supernatants were loaded onto 4–20% Tris-glycine gels. Gels were stained with Coomassie Blue and bands were excised from the gel and analyzed by LC-MS/MS followed by a database search using MASCOT (Proteomics Resource Center, Rockefeller University).

### Microscopy

Growth phase cells were allowed to adhere to MatTek dishes; growth media was then replaced by imaging media (Low Fluorescence Axenic Media, [www.dictybase.org](http://www.dictybase.org)) for several hours before imaging.

Widefield microscopy was performed at the Rockefeller University Bio-Imaging Resource Center (BIRC). A Deltavision Image Restoration Microscope with a 100 $\times$ 1.4 NA objective was used to take Z-slices (200 nm steps), which were deconvolved with the softWoRx software using measured PSFs. Samples were excited with a xenon lamp and either a 490/20 excitation filter, a GFP/mCherry polychroic and a 528/38 emission filter, or a 555/28 excitation filter, a DAPI/FITC/Rhod/Cy5 polychroic and a 685/40 emission filter.

Confocal microscopy was performed at the Rockefeller University BIRC. A Zeiss Axiovert 200 microscope with a Perkin-Elmer Ultraview spinning disk confocal head and a 100 $\times$  1.45 NA objective was used. The laser excitation used was 491 nm with a 491LP dichroic and an ET500LP emission filter; the microscope has an Andor iXon 512 $\times$ 512 EMCCD camera.

TIR-FM: two similar microscopes previously described were used (Mattheyses et al., 2011). A 60 $\times$  1.45 NA objective combined with an additional 1.5  $\times$

magnifier was used. The microscope has a Hamamatsu Orca-ER CCD camera or a Hamamatsu EM-CCD Digital camera C9100. For dual-color imaging, fluorescence emission was collected simultaneously and split into two images using a Cairn OptosplitIII emission splitter. For all TIR-FM imaging, an exposure time of 500 milliseconds was used and images were taken every 1 second for time-lapse imaging or continuously for streaming. For alternating EPI-TIR, images were acquired by changing the angle of incidence of the laser with a pair of galvanometers. A 500-millisecond exposure was used for both EPI and TIR with a delay of ~200 milliseconds between EPI and TIR acquisitions. One set of images was acquired every 1.5 seconds.

### Image analysis

Behavior of GFP-clc or GFP-Ap2A1 puncta: cells were imaged by streaming acquisition and individual puncta were tracked manually for 7.5 seconds and their behavior over this period described. Puncta that disappeared because of cell movement were not included in the analysis.

Duration of GFP-clc or GFP-Ap2A1 on the surface: cells were imaged by time-lapse acquisition and individual puncta were tracked manually or automatically. For manual tracking, the frame of appearance in TIR and disappearance from TIR of individual puncta was used to determine the duration. For automatic tracking, individual puncta were tracked using the 'spots' function in the software Imaris. Criteria for determining spots was manually adjusted for each cell. For tracking, the Brownian motion algorithm was used with a maximum distance of 5 and a gap of 0. The time of appearance in TIR and disappearance from TIR of individual puncta was used to determine the duration.

Statistical analysis: a two-sample Kolmogorov-Smirnov (KS) test was used. The null hypothesis is that the durations are drawn from the same distribution. A nonparametric test was used because the distributions of durations did not correspond to a normal distribution. The test was implemented in Origin 8.5 software.

Number of long-lived puncta: puncta present in the last frame of the time-lapse were tracked and their frame of appearance was determined. Their duration was determined as 'time of last frame' - 'time of appearance in TIR'. The number of puncta with durations over 350 seconds was calculated as a percentage of all the puncta tracked.

Colocalization analysis: for dual-color imaging, red and green fluorescence emission channels were split and aligned using the Cairn Image Splitter Analyzer plugin for ImageJ. A background value of 200 was subtracted from all images followed by using the rolling ball background subtract function (radius 50-100, no smoothing). Single frames from the beginning of time-lapse images were used for colocalization analysis. Manual thresholding was used to outline the puncta for either channel. The maximum intensity pixel within each outline was overlaid onto the outlines of the other channel. A maximum was counted as colocalized if it fell within an outline on the other channel. Percentage overlap was calculated as (number of colocalized maxima/total maxima) × 100. For pixel shift analysis, the outline image was shifted 20 pixels to the left or right in one-pixel increments. The overlap analysis was then performed at each position. Percentage overlap values were calculated for each position and then normalized to the unshifted value. These procedures were implemented via custom macros in ImageJ.

Gaussian fitting: individual puncta were analyzed using a 7 × 7 pixel region excised from the raw data. A custom program was used to fit a 2D, single peak Gaussian to each punctum, the program was implemented in LabView and provided by Dr Daniel Johnson. The width of the Gaussian from the center where it falls to 1/e of the maxima was recorded in X and Y dimensions, the narrowest dimension was used in the measurement (X dimension). Data were compared using a two-sample *t*-test with non-equal variance.

Analysis of individual puncta: puncta were selected for analysis if a fluorescence signal was present in both channels and the puncta disappeared from the TIR field during the time-lapse. For GFP-Ap2A1 and mRFP-clc, puncta were circled in the GFP-Ap2A1 channel and transferred to the clathrin channel. For dajumin-GFP and mRFP-clc, puncta were circled in the mRFP-clc channel and transferred to the dajumin channel. Puncta were tracked using a combination of MATLAB and the ImageJ plugin SpotTracker 2D, as described in Mattheyses et al. (Mattheyses et al., 2011). The average fluorescence intensity of the puncta was measured for both channels and the values normalized to the maximum intensity in each channel for each puncta. The time of initiation of departure was determined for each channel as the point at which the fluorescence intensity of a puncta started to decline irreversibly. Time between AP2 and clathrin disappearance or between dajumin and clathrin disappearance was calculated as 'initiation of departure for mRFP-clc' - 'initiation of departure for GFP-Ap2A1 or dajumin-GFP'.

For EPI versus TIR data, the same analysis was performed as above, puncta centroids were calculated from the GFP-Ap2A1 TIR channel and applied to all other channels. The average fluorescence intensity of the puncta was measured for all channels and the values normalized to the maximum intensity in each channel for each puncta, we then applied a rolling average to the data using a seven-frame window. The time of initiation of appearance was determined for each channel as the point at which fluorescence intensity of a puncta started to increase irreversibly. The time of disappearance was determined as the point at which

there was a plateau in the decline of the fluorescence intensity. Kymographs were created using a maximum intensity projection of the four pixels either side of the center of the spot for every time point. Classification of puncta into various categories was done manually by assessing both the fluorescence intensity measurements and kymographs for each punctum.

### Biotinylation assay

The assay was performed as described in Barth et al. (Barth et al., 1994),  $5 \times 10^6$  cells were used per time point. After the cell surface reduction step, cells were lysed in 50-100  $\mu$ l of lysis buffer and total protein concentration measured. Equal amounts of total protein were used for co-immunoprecipitation as described above, except 10-20  $\mu$ l of GFP-Trap-A beads were used and nutation was performed for 2 hours at 4°C. Samples were eluted from the bead in 30-60  $\mu$ l of non-reducing sample buffer. For detecting GFP, western blots were performed as described above; 5-25  $\mu$ l of the sample was run on a 4-20% Tris-glycine gel followed by transfer to nitrocellulose membranes. For detection of biotin, 20  $\mu$ l of the sample was run on a 4-20% Tris-glycine gel followed by transfer to nitrocellulose membranes. Membranes were blocked for 1 hour with 2% BSA Fraction V in wash buffer (150 mM NaCl, 50 mM Na<sub>2</sub>B<sub>4</sub>O<sub>7</sub>, pH 10.0) and then probed for 1 hour with Pierce High Sensitivity Streptavidin-HRP (1:8,000) in 4% BSA Fraction V in wash buffer containing 0.02% Triton-X100. Membranes were washed three times with wash buffer containing 0.01% Triton-X100, followed by three washes with wash buffer containing 0.1% Triton-X100. HRP was visualized using ECL Plus.

### Immunofluorescence

Cells were incubated in imaging media on 25 mm NO. 1.5 glass coverslips and fixed as described in (Fok et al., 1993) but without the agar overlay. Cells were then immunostained (Clarke et al., 1987) with the N4 antibody (Fok et al., 1993) (1:50) followed by a goat anti-mouse AF488 secondary antibody (1:400). Z-slices were taken with a widefield microscope with a 100 × 1.35 NA objective and deconvolved with the software Huygens using calculated PSFs. Samples were excited with a xenon lamp and a 470/40 excitation filter, a GFP dichroic mirror was used with a 520/40 emission filter.

### FM4-64 staining

Cells were incubated in imaging media on MatTek dishes and FM4-64 dye was added at 1  $\mu$ g/ml for 20 min. Cells were imaged with the Deltavision microscope described above.

### Acknowledgements

We thank Dr T O'Halloran and Dr A. Müller-Taubenberger for reagents. We thank The Rockefeller University BIRC and Proteomics Resource Center, Dr Marina Fix for manuscript editing and Dr Daniel Johnson for the Gaussian fitting program.

### Funding

This work was funded the National Institutes of Health (National Institute of General Medical Sciences) [grant number 5R01GM087977-03 to S.M.S.]. L.M. is supported by the Boehringer Ingelheim Fonds. Deposited in PMC for release after 12 months.

Supplementary material available online at

<http://jcs.biologists.org/lookup/suppl/doi:10.1242/jcs.108837/-/DC1>

### References

- Barth, A., Müller-Taubenberger, A., Taranto, P. and Gerisch, G. (1994). Replacement of the phospholipid-anchor in the contact site A glycoprotein of *D. discoideum* by a transmembrane region does not impede cell adhesion but reduces residence time on the cell surface. *J. Cell Biol.* **124**, 205-215.
- Bennett, N., Letourneur, F., Ragno, M. and Louwagie, M. (2008). Sorting of the v-SNARE VAMP7 in *Dictyostelium discoideum*: a role for more than one Adaptor Protein (AP) complex. *Exp. Cell Res.* **314**, 2822-2833.
- Boucrot, E., Saffarian, S., Zhang, R. and Kirchhausen, T. (2010). Roles of AP-2 in clathrin-mediated endocytosis. *PLoS ONE* **5**, e10597.
- Brady, R. J., Wen, Y. and O'Halloran, T. J. (2008). The ENTH and C-terminal domains of *Dictyostelium* epsin cooperate to regulate the dynamic interaction with clathrin-coated pits. *J. Cell Sci.* **121**, 3433-3444.
- Brady, R. J., Damer, C. K., Heuser, J. E. and O'Halloran, T. J. (2010). Regulation of Hip1r by epsin controls the temporal and spatial coupling of actin filaments to clathrin-coated pits. *J. Cell Sci.* **123**, 3652-3661.
- Clarke, M., Kayman, S. C. and Riley, K. (1987). Density-dependent induction of discoidin-I synthesis in exponentially growing cells of *Dictyostelium discoideum*. *Differentiation* **34**, 79-87.
- Collins, B. M., McCoy, A. J., Kent, H. M., Evans, P. R. and Owen, D. J. (2002). Molecular architecture and functional model of the endocytic AP2 complex. *Cell* **109**, 523-535.

- Ehrlich, M., Boll, W., Van Oijen, A., Hariharan, R., Chandran, K., Nibert, M. L. and Kirchhausen, T. (2004). Endocytosis by random initiation and stabilization of clathrin-coated pits. *Cell* **118**, 591-605.
- Fischer, M., Haase, I., Simmeth, E., Gerisch, G. and Müller-Taubenberger, A. (2004). A brilliant monomeric red fluorescent protein to visualize cytoskeleton dynamics in Dictyostelium. *FEBS Lett.* **577**, 227-232.
- Fok, A. K., Clarke, M., Ma, L. and Allen, R. D. (1993). Vacuolar H<sup>+</sup>-ATPase of Dictyostelium discoideum. A monoclonal antibody study. *J. Cell Sci.* **106**, 1103-1113.
- Gabriel, D., Hacker, U., Köhler, J., Müller-Taubenberger, A., Schwartz, J. M., Westphal, M. and Gerisch, G. (1999). The contractile vacuole network of Dictyostelium as a distinct organelle: its dynamics visualized by a GFP marker protein. *J. Cell Sci.* **112**, 3995-4005.
- Gerisch, G., Heuser, J. and Clarke, M. (2002). Tubular-vesicular transformation in the contractile vacuole system of Dictyostelium. *Cell Biol. Int.* **26**, 845-852.
- Henne, W. M., Boucrot, E., Meinecke, M., Evergren, E., Vallis, Y., Mittal, R. and McMahon, H. T. (2010). FCHO proteins are nucleators of clathrin-mediated endocytosis. *Science* **328**, 1281-1284.
- Heuser, J. (2006). Evidence for recycling of contractile vacuole membrane during osmoregulation in Dictyostelium amoebae—a tribute to Günther Gerisch. *Eur. J. Cell Biol.* **85**, 859-871.
- Heuser, J., Zhu, Q. and Clarke, M. (1993). Proton pumps populate the contractile vacuoles of Dictyostelium amoebae. *J. Cell Biol.* **121**, 1311-1327.
- Huang, K. M., D'Hondt, K., Riezman, H. and Lemmon, S. K. (1999). Clathrin functions in the absence of heterotetrameric adaptors and AP180-related proteins in yeast. *EMBO J.* **18**, 3897-3908.
- Keyel, P. A., Watkins, S. C. and Traub, L. M. (2004). Endocytic adaptor molecules reveal an endosomal population of clathrin by total internal reflection fluorescence microscopy. *J. Biol. Chem.* **279**, 13190-13204.
- Lefkir, Y., de Chasse, B., Dubois, A., Bogdanovic, A., Brady, R. J., Destaing, O., Bruckert, F., O'Halloran, T. J., Cosson, P. and Letourneur, F. (2003). The AP-1 clathrin-adaptor is required for lysosomal enzymes sorting and biogenesis of the contractile vacuole complex in Dictyostelium cells. *Mol. Biol. Cell* **14**, 1835-1851.
- Lemmon, S. K. and Jones, E. W. (1987). Clathrin requirement for normal growth of yeast. *Science* **238**, 504-509.
- Matheyses, A. L., Atkinson, C. E. and Simon, S. M. (2011). Imaging single endocytic events reveals diversity in clathrin, dynamin and vesicle dynamics. *Traffic* **12**, 1394-1406.
- McMahon, H. T. and Boucrot, E. (2011). Molecular mechanism and physiological functions of clathrin-mediated endocytosis. *Nat. Rev. Mol. Cell Biol.* **12**, 517-533.
- Mercanti, V., Blanc, C., Lefkir, Y., Cosson, P. and Letourneur, F. (2006a). Acidic clusters target transmembrane proteins to the contractile vacuole in Dictyostelium cells. *J. Cell Sci.* **119**, 837-845.
- Mercanti, V., Charette, S. J., Bennett, N., Ryckewaert, J.-J., Letourneur, F. and Cosson, P. (2006b). Selective membrane exclusion in phagocytic and macropinocytic cups. *J. Cell Sci.* **119**, 4079-4087.
- Merrifield, C. J., Feldman, M. E., Wan, L. and Almers, W. (2002). Imaging actin and dynamin recruitment during invagination of single clathrin-coated pits. *Nat. Cell Biol.* **4**, 691-698.
- Merrifield, C. J., Perrais, D. and Zenisek, D. (2005). Coupling between clathrin-coated-pit invagination, cortactin recruitment, and membrane scission observed in live cells. *Cell* **121**, 593-606.
- Motley, A., Bright, N. A., Seaman, M. N. J. and Robinson, M. S. (2003). Clathrin-mediated endocytosis in AP-2-depleted cells. *J. Cell Biol.* **162**, 909-918.
- Niswonger, M. L. and O'Halloran, T. J. (1997a). Clathrin heavy chain is required for spore cell but not stalk cell differentiation in Dictyostelium discoideum. *Development* **124**, 443-451.
- Niswonger, M. L. and O'Halloran, T. J. (1997b). A novel role for clathrin in cytokinesis. *Proc. Natl. Acad. Sci. USA* **94**, 8575-8578.
- O'Halloran, T. J. and Anderson, R. G. (1992). Clathrin heavy chain is required for pinocytosis, the presence of large vacuoles, and development in Dictyostelium. *J. Cell Biol.* **118**, 1371-1377.
- Ohno, H., Stewart, J., Fournier, M. C., Bosshart, H., Rhee, I., Miyatake, S., Saito, T., Gallusser, A., Kirchhausen, T. and Bonifacino, J. S. (1995). Interaction of tyrosine-based sorting signals with clathrin-associated proteins. *Science* **269**, 1872-1875.
- Owen, D. J., Collins, B. M. and Evans, P. R. (2004). Adaptors for clathrin coats: structure and function. *Annu. Rev. Cell Dev. Biol.* **20**, 153-191.
- Page, L. J. and Robinson, M. S. (1995). Targeting signals and subunit interactions in coated vesicle adaptor complexes. *J. Cell Biol.* **131**, 619-630.
- Payne, G. S. and Schekman, R. (1985). A test of clathrin function in protein secretion and cell growth. *Science* **230**, 1009-1014.
- Praefcke, G. J. K., Ford, M. G. J., Schmid, E. M., Olesen, L. E., Gallop, J. L., Peak-Chew, S.-Y., Vallis, Y., Babu, M. M., Mills, I. G. and McMahon, H. T. (2004). Evolving nature of the AP2 alpha-appendage hub during clathrin-coated vesicle endocytosis. *EMBO J.* **23**, 4371-4383.
- Rappoport, J. Z., Taha, B. W., Lemeer, S., Benmerah, A. and Simon, S. M. (2003). The AP-2 complex is excluded from the dynamic population of plasma membrane-associated clathrin. *J. Biol. Chem.* **278**, 47357-47360.
- Rappoport, J. Z., Benmerah, A. and Simon, S. M. (2005). Analysis of the AP-2 adaptor complex and cargo during clathrin-mediated endocytosis. *Traffic* **6**, 539-547.
- Rappoport, J. Z., Kemal, S., Benmerah, A. and Simon, S. M. (2006). Dynamics of clathrin and adaptor proteins during endocytosis. *Am. J. Physiol. Cell Physiol.* **291**, C1072-C1081.
- Repass, S. L., Brady, R. J. and O'Halloran, T. J. (2007). Dictyostelium Hip1r contributes to spore shape and requires epsin for phosphorylation and localization. *J. Cell Sci.* **120**, 3977-3988.
- Ruscetti, T., Cardelli, J. A., Niswonger, M. L. and O'Halloran, T. J. (1994). Clathrin heavy chain functions in sorting and secretion of lysosomal enzymes in Dictyostelium discoideum. *J. Cell Biol.* **126**, 343-352.
- Shih, W., Gallusser, A. and Kirchhausen, T. (1995). A clathrin-binding site in the hinge of the beta 2 chain of mammalian AP-2 complexes. *J. Biol. Chem.* **270**, 31083-31090.
- Sosa, R. T., Weber, M. M., Wen, Y. and O'Halloran, T. J. (2012). A single  $\beta$  adaptin contributes to AP1 and AP2 complexes and clathrin function in Dictyostelium. *Traffic* **13**, 305-316.
- Stavrou, I. and O'Halloran, T. J. (2006). The monomeric clathrin assembly protein, AP180, regulates contractile vacuole size in Dictyostelium discoideum. *Mol. Biol. Cell* **17**, 5381-5389.
- van Delft, S., Schumacher, C., Hage, W., Verkleij, A. J. and van Bergen en Henegouwen, P. M. (1997). Association and colocalization of Eps15 with adaptor protein-2 and clathrin. *J. Cell Biol.* **136**, 811-821.
- Veltman, D. M., Akar, G., Bosgraaf, L. and Van Haastert, P. J. M. (2009). A new set of small, extrachromosomal expression vectors for Dictyostelium discoideum. *Plasmid* **61**, 110-118.
- Wang, J., Virta, V. C., Riddelle-Spencer, K. and O'Halloran, T. J. (2003). Compromise of clathrin function and membrane association by clathrin light chain deletion. *Traffic* **4**, 891-901.
- Wang, J., Wang, Y. and O'Halloran, T. J. (2006). Clathrin light chain: importance of the conserved carboxy terminal domain to function in living cells. *Traffic* **7**, 824-832.
- Wen, Y., Stavrou, I., Bersuker, K., Brady, R. J., De Lozanne, A. and O'Halloran, T. J. (2009). AP180-mediated trafficking of Vamp7B limits homotypic fusion of Dictyostelium contractile vacuoles. *Mol. Biol. Cell* **20**, 4278-4288.
- Yeung, B. G., Phan, H. L. and Payne, G. S. (1999). Adaptor complex-independent clathrin function in yeast. *Mol. Biol. Cell* **10**, 3643-3659.